archives
of thermodynamics
Vol. **32**(2011), No. 1, 3–20
DOI: 10.2478/v10173-011-0001-9

Multifractal properties of large bubble paths in a single bubble column

ROMUALD MOSDORF*
TOMASZ WYSZKOWSKI
KAMIL KAROL DĄBROWSKI

Bialystok Technical University, Faculty of Mechanical Engineering, Wiejska 45C, 15-351 Białystok, Poland

Abstract In the paper the paths of bubbles emitted from the brass nozzle with inner diameter equal to 1.6 mm have been analyzed. The mean frequency of bubble departure was in the range from 2 to 65.1 Hz. Bubble paths have been recorded using a high speed camera. The image analysis technique has been used to obtain the bubble paths for different mean frequencies of bubble departures. The multifractal analysis (WTMM – wavelet transform modulus maxima methodology) has been used to investigate the properties of bubble paths. It has been shown that bubble paths are the multifractals and the influence of previously departing bubbles on bubble trajectory is significant for bubble departure frequency $f_b > 30$ Hz.

Keywords: Bubble column; Bubble dynamics; WTMM method

Nomenclature

a_1, a_2, ..., a_n	–	coefficients in Taylor series
C	–	constant
d	–	bubble diameter, m
D_h	–	global singularity spectrum
f	–	function
H	–	Hurst exponent

*Corresoponding author. E-mail address: r.mosdorf@pb.edu.pl

h – Hölder exponent
N – number of considered states
P_n – n-th order polynomial
q – q-th moment
s – scale parameter
x – samples value
X – time series
Y – time series
W – wavelet transform
Z – partition function

Greek symbols

$\Omega(s)$ – sum of all maxima over scale s
$\tau(q)$ – scaling exponent
$\psi(x)$ – wavelet function

Subscripts

e – equivalent sphere diameter
h – Hölder exponent
o – initial value
n – order

1 Introduction

Bubble-fluid interactions are significant in many technological applications such as bubble column reactors, oil/natural gas transport, boiling heat transfer, etc. The study of bubble dynamics is crucial to understand bubble--liquid and bubble-bubble interactions. According to [1] the bubble motion and bubble shape are controlled by deterministic forces such as body force and drag force caused by the convective motion, and the complex non-linear forces generated by liquid motion around bubbles. Results of investigation show that such parameters as: bubble departure frequency (time between subsequent departing bubbles), bubble departure diameter, bubble shape and its deformation, gas pressure fluctuation in the nozzle, bubbles interaction, bubbles coalescence and bouncing, liquid flow pattern around the bubbles and bubble column change in time chaotically [2–6].

The tubes of streamwise liquid vorticity are being left by each bubble and they are responsible for the appearance of lift force acting on the bubbles [7]. The strength of the circulation of each vortex tubes decreases with increase in the distance from the bubble. Therefore bubbles in the bubble column create the complex structure of bubble wakes. These wakes interact between each others and finally modify the bubbles trajectory. The increase

of bubble departure frequency decreases the vertical distance between bubbles. It causes the increase of interaction between the bubbles and tubes of streamwise liquid vorticity generated by previously departed bubbles. Such interaction changes the lift force and finally modifies the oscillation bubble trajectory.

In the present paper the dynamical properties of bubble paths have been investigated to detect the intensity of interaction of bubbles with the structure of liquid flow in the bubble column. The paths of bubbles emitted from the brass nozzle with inner diameter equal to 1.6 mm has been analyzed. The bubble departure diameter was ∼4.6 mm. The laser-photodiode system has been used to measure the bubble departures frequency. The analyzed frequencies ranged from 2 Hz to 65.1 Hz (bubbles per second). The bubble paths have been recorded using a high speed camera. The image analysis technique enabled obtaining the bubble paths for different mean frequencies of bubble departures. The multifractal analysis (WTMM – wavelet transform modulus maxima methodology) has been used to investigate properties of bubble paths in the bubble column. It has been shown that multifractal analysis allows to recognize the changes of dynamics of bubble flow depending on the bubble departure frequency.

2 Experimental setup

The air bubble paths in bubble column in the tank ($400\times500\times40$ mm) filled with distilled water have been investigated. In the experiment bubbles were generated from the brass nozzle with inner diameter of 1.6 mm. The mean bubble departure diameter was estimated using the set of obtained photos with resolution ∼100 pixels per one millimeter and it was about 4.6 mm.

Because in the experiment with bubble column generation both the pressure and gas mass flux fluctuated then in order to evaluate experiment conditions it was necessary to use the mean value of gas mass flux or bubble departure frequency. In the present experiment the mean bubble departure frequency was used as a control parameter. The frequency has been measured using simultaneously the laser-phototransistor system and gas pressure sensor. The gas pressure fluctuation has been measured using uncompensated silicon pressure sensor MPX12DP. In the laser-phototransistor system the semiconductor red laser with the wave length of 650 nm, 3 mW, special aperture and phototransistor BPYP22 has been used. The diameter of laser ray was 0.2 mm. The experiment has been carried out in conditions

when subsequent departing bubbles did not coalesce vertically close to the nozzle outlet. The frequency of bubble departure was in the range from 2 to 65.1 bubbles per second, the water temperature was 20 °C.

All data was simultaneously recorded using the data acquisition system DT9800 series USB Function Modules for Data Acquisition Systems with sampling frequency of 1000 Hz. The air supply system consisted of air tank capacity of 2 dm^3 and the electronically controlled air pump, where the velocity of electric engine was controlled by the chip U2008B. The scheme of experimental stand has been shown in Fig. 1.

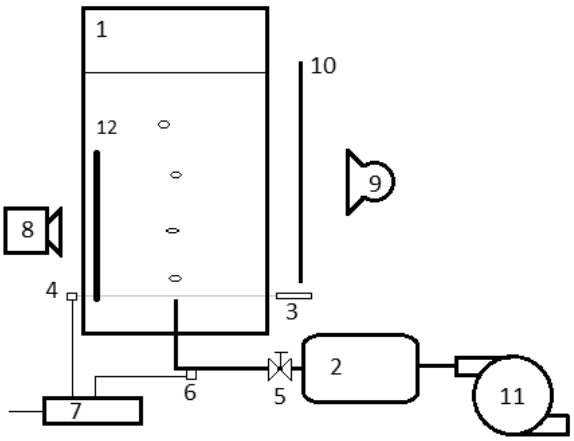

Figure 1. Experimental setup: 1 – glass tank (400 mm×500 mm×40 mm), 2 – air tank, 3 – laser, 4 – phototransistor, 5 – air valve, 6 – pressure sensor, 7 – computer acquisition system (DT9800 series USB Function Modules for Data Acquisition Systems), 8 – Casio EX FX1(600 fps), 9 – light source, 10 – screen, 11 – air pump with electronic control, 12 – the rectangle area of 230×50 mm where the bubble paths have been recorded.

Bubble paths have been recorded in the rectangle area of 230 mm×50 mm using the high speed camera Casio EX FX1. The recorded color video (600 fps) has been divided into frames. All colored frames ware converted into gray scale images. The Sobel filter based on convolution of the image with a small, integer valued filter has been used to identify the bubbles on the frames [8]. Exemplary results of using the Sobel filter for bubble image are presented in Fig. 2a. Because the Sobel algorithm identifies only the edge of the bubble, therefore the additional algorithm to fill interior of the detected bubble by black pixels has been used. Finally, each bubble was

visible in the frame as a set of black pixels (Fig. 2).

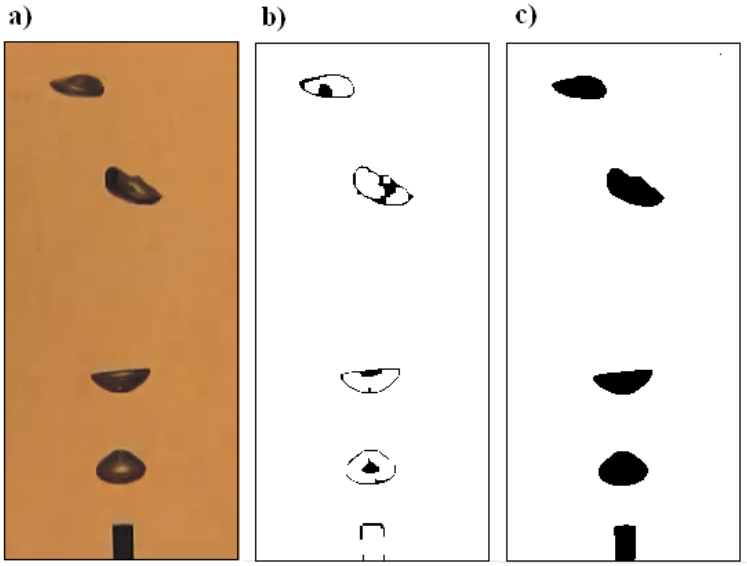

Figure 2. The bubble identification process: a) original photo, b) results of Sobel filter, c) filling interior of the bubbles by black pixels.

The path of each bubble was reconstructed by tracking the trajectory of mass center of each bubble in subsequent frames. The mass centre has been calculated according to the following formula:

$$x_c = \frac{\Sigma_i \Sigma_j k}{s}, \quad \text{where} \quad k = \begin{cases} i & \text{for black pixels,} \\ 0 & \text{otherwise,} \end{cases} \tag{1}$$

$$y_c = \frac{\Sigma_i \Sigma_j k}{s}, \quad \text{where} \quad k = \begin{cases} j & \text{for black pixels,} \\ 0 & \text{otherwise,} \end{cases} \tag{2}$$

where s denotes the area of the bubble picture.

3 Bubble behaviors

3.1 Previous works

The bubble size is one of the factors which determines the shape of the bubble path. A number of experimental and numerical studies have been carried out to investigate the movement of single millimeter-sized air bubble

in water [9]. Those investigations show that for $d_e < 1$ mm the bubble path is similar to a vertical line. For $d_e > 1$ the bubble at first flows along the vertical line and then it develops a zigzag motion, which in certain conditions changes into a spiraling circular motion. Bubble path instabilities occur when the Reynolds number is greater than 10^3. The problem of the bubble path shape and its instability has been considered in the papers [7,10–16]. In the paper [17] the paths of bubbles for different initial bubble diameters have been analyzed. It has been shown that the function of mean lateral displacement of the bubble versus equivalent sphere diameter of the bubble has two maxima. The first one (for $d_e \sim 2$ mm) appears when the bubble path is similar to periodic function and the other one (for $d_e \sim 4$ mm) when the random lateral displacement of the bubble is observed. The mean frequency of bubble lateral displacement is independent of the bubble size and it is equal to ∼5 Hz [17].

In the paper [18] the bubble shape oscillations have been analyzed. The initial bubble diameter was 3.4 mm and its departure frequency was 5 Hz. It has been found that when the bubbles flatten then their paths become more sensitive to perturbations. In this experiment the bubbles continue a rectilinear rise for 25 mm above the nozzle outlet. At this position, the bubble aspect ratio reaches the value of ≈3.15. At the same time the complex shape oscillations and path transition to a spiral form occur. In the paper [1] changes of rise velocity, the shape and orientation of bubbles were simultaneously measured using a high-speed camera. Investigations have been carried out in the channel whose cross section was 100 mm×7 mm×600 mm. Bubbles have been produced from the nozzle with inner diameter equal to 4 mm. The chaotic fluctuation of bubble shape and its rise velocity have been observed. The fluctuation in bubble rise velocity can be considered as a consequence of oscillation of drag force associated with the bubble-shape fluctuation. In the paper [19] the movement of two bubbles with a radius of 0.41 mm to 0.95 mm has been investigated. The initial distance between bubbles was in the range from 2.2 mm to 5.0 mm. It has been found that the patterns of the trajectories of rising bubbles are strongly dependent on the Reynolds number. When the Reynolds number is over the critical region, two bubbles approach each other and then they collide. After the collision, two types of motions are observed. These are the coalescence and bouncing. The velocities of bubbles decrease by ∼50% when the bubbles bounce with each other. It has been observed that the behavior of repeatedly bouncing bubbles is significantly influenced by the wake instability of a single bubble

rather than by bubble-bubble interaction.

In the paper [20] it has been shown that bubbles rise in approximately identical trajectories up to the distance less than 40 mm from the nozzle outlet. In the experiment d_e was in the range of 0.66–2.0 mm The distance of bubble trajectories from the vertical axis increases together with the increase of bubble departure frequency. In the paper [21] it has also been shown using the PIV technique that the variation of bubble rising trajectory and bubble shape is closely associated with liquid viscosity but less related to the frequency of bubble formation. The bubble departure diameter was about 6 mm. It has been observed that bubble rising trajectory changes from a rectilinear path to a zigzag and spiral path as liquid viscosity reduces.

In the paper [7] the phenomena responsible for the appearance of the bubble oscillatory trajectory have been analyzed using the PIV technique. It has been shown that the transition to oscillatory trajectory of bubble is connected with appearance of two vortex tubes of streamwise vorticity behind the bubble. It appears that when the bubble aspect ratio exceeds a critical value (for large Reynolds number) the wake becomes unstable and induces a horizontal force acting on the bubble. It has been found that the zigzagging motion occurs in a plane which separates the two vortex tubes and the magnitude of horizontal force is equal to 20–30% of the buoyancy force.

In the paper [22,23] the dynamics in the wake of a circular disk and sphere embedded in an uniform flow has been investigated using DNS. It has been shown that when the Reynolds number increases then the original series of bifurcations leading to chaos appears in the flow. In the paper [24] the model based on the generalized Kirchhoff equations and dynamical model of the wake deduced from experimental observations has been presented. The model generates the oscillatory paths observed in the experiment.

3.2 Experimental results

In Fig. 3 it has been shown the data recorded from the phototransistor and pressure sensor for different mean frequencies of bubble departures. The laser ray passed 3 mm above the nozzle outlet. When the bubble was passing through the laser ray the phototransistor sensor generated the signal of the low voltage level. The time between bubbles is visible in Fig. 3 as a signal of the high voltage level. Obtained results show that for all frequencies of bubble departures the time periods in which the bubbles pass through the laser ray are approximately the same, but time periods between

subsequent departing bubbles decrease together with increase of bubble departure frequency. For bubble departure frequency equal to 65.1 Hz (Fig. 3f) time periods between bubbles are shorter that time periods when bubbles pass through the laser ray. When bubbles depart, the air pressure rapidly decreases as it has been shown in Fig. 3. It has been found that both the maximum pressure when bubble starts to grow and minimum pressure when bubble departs vary in time for bubble departure frequencies higher than 14 Hz. The number of minima of pressure signal and number of periods with low voltage level signal coming from phototransistor sensor have been used to determine bubble departure frequencies.

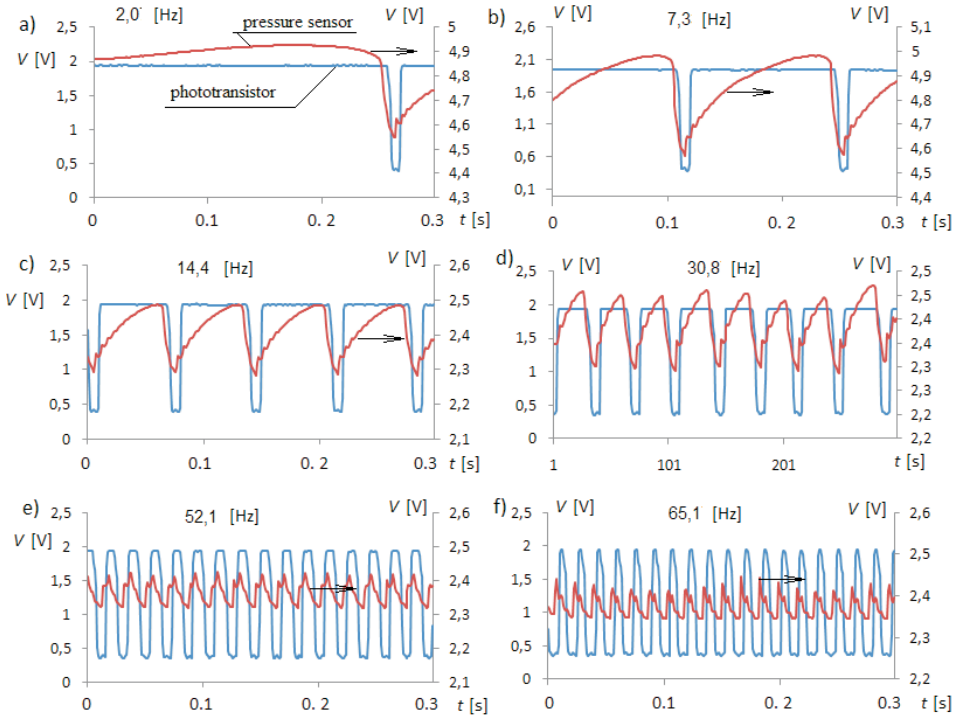

Figure 3. Pressure and phototransistor signal recorded for different frequencies of bubble departures f_b: a) $f_b = 2$ Hz, b) $f_b = 7.3$ Hz, c) $f_b = 14.4$ Hz, d) $f_b = 30.08$ Hz, e) $f_b = 52.1$ Hz, f) $f_b = 65.1$ Hz.

In Fig. 4 the typical behavior of bubble flow for different mean bubble departure frequencies has been presented. Below each of images it has been presented the example of changes in time of horizontal position of one

selected bubble in each column. Time series have been recorded during different time periods because time of passing bubbles through the rectangle area (where video has been recorded) depends on vertical velocities of bubbles, while the velocities depend on the bubble departure frequencies.

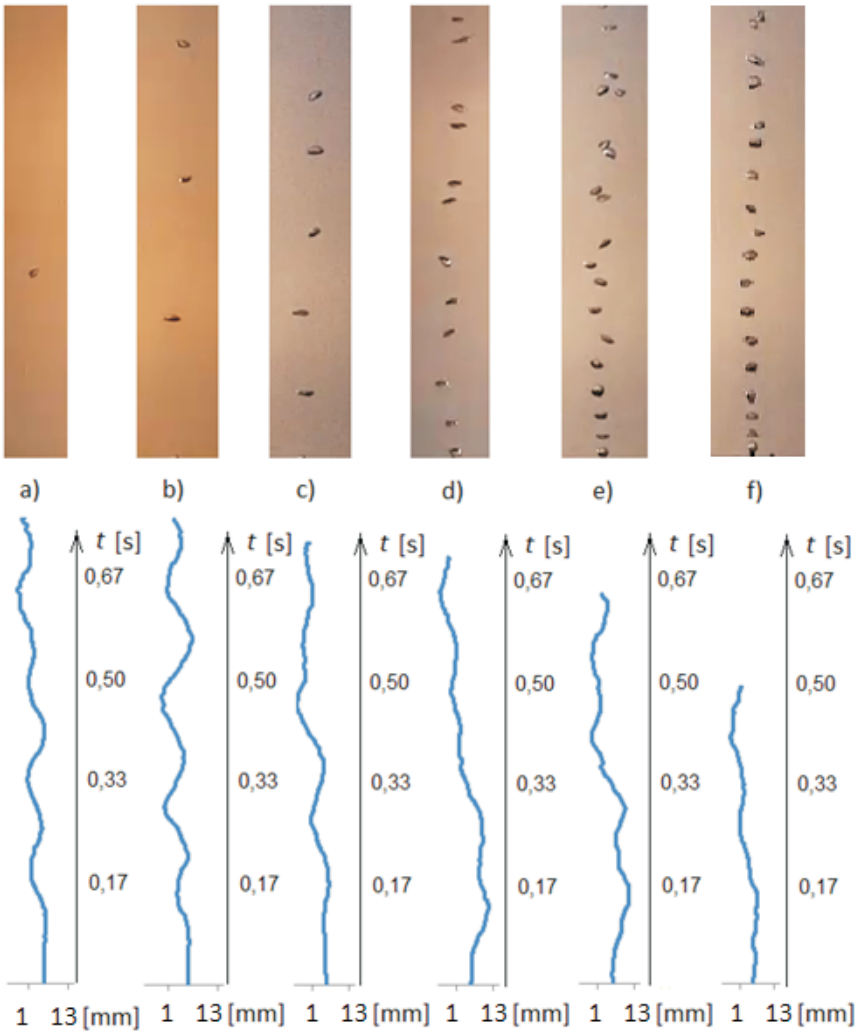

Figure 4. Changes in time of the bubble horizontal position and the typical behavior of bubble flow for different mean bubble departure frequencies f_b: a) $f_b = 2$ Hz, b) $f_b = 7.3$ Hz, c) $f_b = 14.4$ Hz, d) $f_b = 30.08$ Hz, e) $f_b = 52.1$ Hz, f) $f_b = 65.1$ Hz.

For the low bubble departure frequency (2 Hz) the length of almost rectilinear path (with a small lateral bubble displacement) was equal to ∼26 mm and it decreased together with increasing bubble departure frequency up to ∼13 mm for $f_b = 52.1$ Hz (Fig. 4e). The bubble deformation in almost rectilinear, bubble motion had a periodic character and it repeated for subsequent bubbles. In Fig. 5 it has been shown the typical bubble deformation during the rectilinear movement for $f_b = 14.1$ Hz. Subsequent figures present the bubble deformation in different stages. The arrows show the stages of the bubble when it flows in the bubble column. The rectilinear path finishes between Figs. 5c and 5d, where the rapid irregular bubble deformation starts.

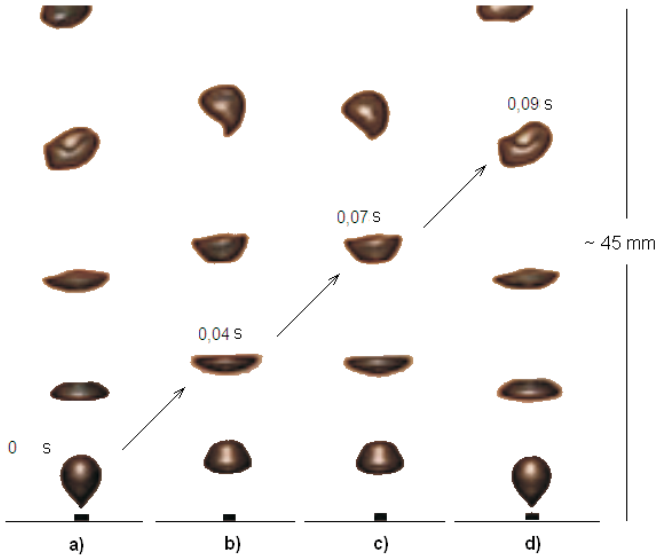

Figure 5. Typical deformation of bubble during its rectilinear movement, the arrows show subsequent stages of the bubble during its flow in the column. The frequency of bubble departure was equal to 14.4 Hz.

The analysis of movement of mass centre of bubbles allows us to estimate the mean vertical terminal velocity of bubble in the column as a function of mean bubble departure frequency. In Fig. 6a it has been shown the changes of vertical velocity of bubble. After the bubble departure its vertical velocity increases and reaches the terminal value. Oscillations of vertical velocity around the terminal velocity are connected with the oscillatory movement of the bubble. The mean terminal vertical velocity has been calculated during

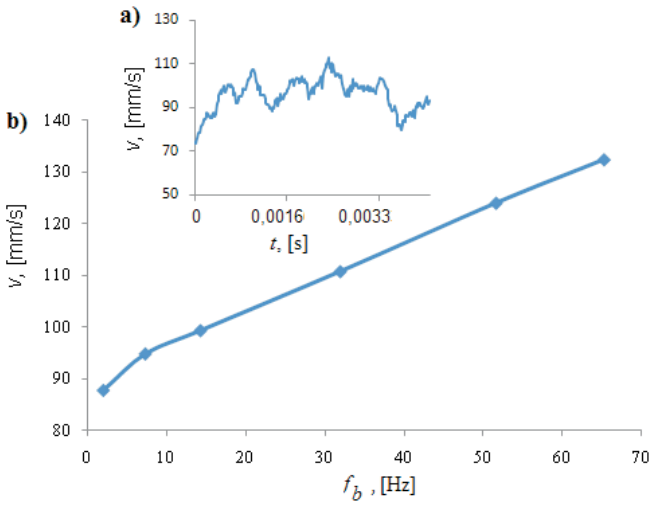

Figure 6. Terminal vertical velocity of bubbles in bubble column. a) Changes of vertical velocity of bubble for $f_b = 14.4$ Hz. b) Mean vertical bubble velocity versus bubble departure frequency. Calculation has been made for trajectory presented in Fig. 4.

the time period from 0.0016 to 0.0033 s. It increases together with increase in frequency of bubble departure (Fig. 6b).

4 Multifractal analysis

The multifractal analysis can be used to classify time series singularities. In this case the singularity is a rapid change of series values in the small time period. In the times where singularities are presented, the expansion of the time series contains some components with non-integer powers of time. Time series around the singularity point t_0 is represented as [25]:

$$f(t) = a_0 + a_1 + a_1(t - t_0) + \ldots + a_1(t - t_0)^n + C|t - t_0|^\alpha \, . \tag{3}$$

The exponent $h(t_0)$ is called the local Hölder exponentand for t_0 it is defined as the greatest value of α that satisfies the condition [25]:

$$|f(t) - P_n(t - t_0)| \leq C|t - t_0|^{h(t_0)}) \, , \tag{4}$$

$$h(t_0) = sup\{\alpha : f \in C^\alpha(t_0)\} \, . \tag{5}$$

The local Hölder exponent is a measure of strength of the singularity and the regularity of the time series at t_0. The lower value of Hölder exponent is characteristic for the stronger singularity. The Hölder exponent which is a measure of the singularity strength can be considered as a local version of the Hurst exponent [26] and is calculated as $H = h - 1$. In case of monofractal time series, when H is equal to 0.5, the series is random, which means that its subsequent samples are not correlated. When $0 < H < 0.5$ the series is called the ergodic series (its subsequent values oscillates around the mean value). The series becomes more ergodic when the Hurst exponent approaches to zero. For $0.5 < H < 1$ the series amplifies the trend. In this kind of series, e.g. when a certain element of series is above the mean value, it is probable that the next element will also be above the mean value. In such series the trend is visible.

One of methods for Hölder exponent calculation is based on the wavelet transform [27,28]. The wavelet transform filters out the polynomial trends and focuses only on the singularities in the time series. A power law proportionality between the Hölder exponent and wavelet transform is as follows [27,28]:

$$W_{s,x_0}(f) \sim s^{h(x_0)} \text{ for } s \to 0^+ , \tag{6}$$

where $W_{s,x_0}(f) = \frac{1}{s}\int_{-\infty}^{+\infty} \psi(\frac{x-x_0}{s}) f(x)dx$ is a walvlet transform, $\psi(x)$ is a wavelet function orthogonal to the polynomial $f(x)$ up to order n, and s is a scale defining the width (frequency) of wavelet.

The Hölder exponent is estimated using the partition function $Z(s,q)$ that is calculated based on the maximum lines of wavelet transform [28]. The definition of the partition function $Z(s,q)$ of q-th moment based on multifractal formalism is as follows [28]:

$$Z(s,q) = \Sigma_{\Omega(s)} |W_{s,x_)}(f)|^q \alpha s^{\tau(q)} , \tag{7}$$

where $\Omega(s)$ is the sum of all maxima over the scale s, and $r(q)$ is the scaling exponent that characterizes the power law behavior of this partition function. The Legendre transform of $\tau(q)$ defines a relationship between itself and global singularity spectrum D_h [28]:

$$h(q) = \frac{d\tau(q)}{dq} , \tag{8}$$

$$D_h = qh(q) - \tau(q) , \tag{9}$$

where $h(q)$ is the global distribution of Hölder exponents defined at the moment q.

The negative values of q stresses the weak exponents, whereas the positive values stresses the stronger exponents. The D_h spectrum provides us with estimation of global singularities of the time series. This spectrum corresponds to frequency distribution of measure of certain physical quantities over the geometrical set. The 3rd derivation of Gauss function with a form:

$$\psi(t) = \left[\exp\left(\frac{-t^2}{2}\right)\right]''' \tag{10}$$

has been used in WTMM analysis of bubble lateral displacements. In Fig. 7 the example of WTMM analysis of bubble paths has been presented. The wavelet transform of bubble path has been shown in Fig. 7a and the WTMM tree (location of local maximum of wavelet transform) is visible in Fig. 7b.

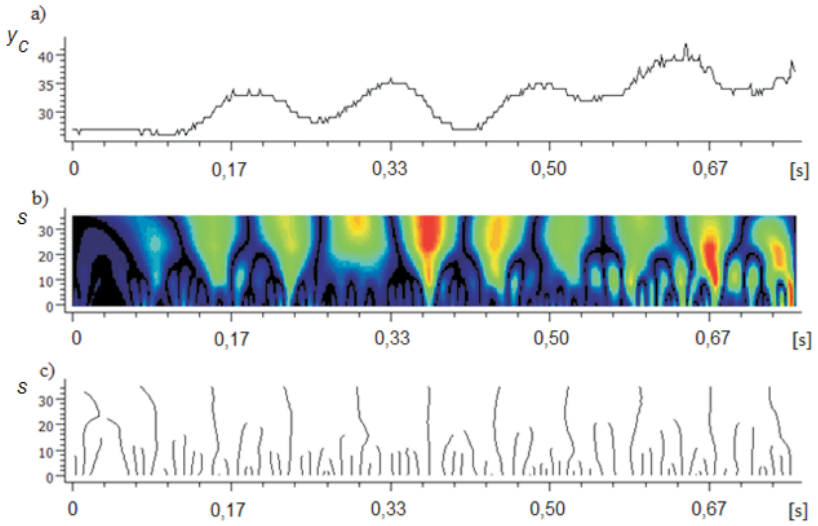

Figure 7. The wavelet transform modulus maxima (WTMM) of bubble path for frequency of bubble departure equal to 2 Hz: a) bubble path, b) wavelet transform of bubble path, c) wavelet transform modulus maxima (WTMM tree). The calculation has been made using the libraries of LastWave [29,30] for trajectory presented in Fig. 4.

The WTMM tree has been used to calculate the spectrum of local Hölder exponent. The multufractal spectrum of lateral bubble displacement in case of frequency of bubble departure equal to 2 Hz is shown in Fig. 8a. The calculation has been made using the libraries of LastWave [29,30]. The function D_h changes within a relatively wide range of h, therefore we can

conclude that the bubble path has a multifractal character. The value of h_{max} characterizes the process of small scale oscillations, whereas the value of h_{min} characterizes the process of large scale fluctuation of lateral bubble displacements. The value of h_{max} close to 2 would suggest a non-random, correlated behavior at small scales horizontal displacements of bubbles. The value of h_{Dmax} is characteristic for the entire process of bubbles flow. This process is a sum of large and small scale displacements of bubbles. The difference between values $(h_{max} - h_{min})$ is a measure of multifractal properties of bubble paths. In Fig. 8b the values of $(h_{max} - h_{min})$ versus mean frequencies of bubble departure have been shown. Obtained results show that in all cases under consideration the bubble lateral displacements have multifractal character and for higher frequency of bubble departure the multifractal properties are clearly visible.

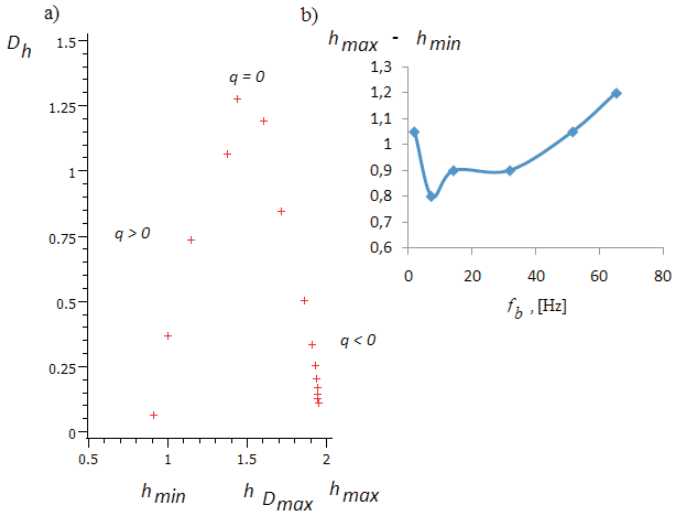

Figure 8. The singularity spectrum. a) The singularity spectrum for bubble trajectory for frequency of bubble departure equal to 2 Hz. b) The measure of multifractal character of bubble paths versus bubble departure frequency. Calculation has been made using the libraries in LastWave [29,30] for trajectory presented in Fig. 4.

In Fig. 9 it has been shown the changes of mean values of Hurst exponent $H_{Dmax} = h_{Dmax} - 1$ vs frequencies of bubble departures. The mean value has been calculated for five trajectories obtained for different mean frequencies of bubble departures. In Fig. 9 the maximum and minimum values of H_{Dmax} have been presented.

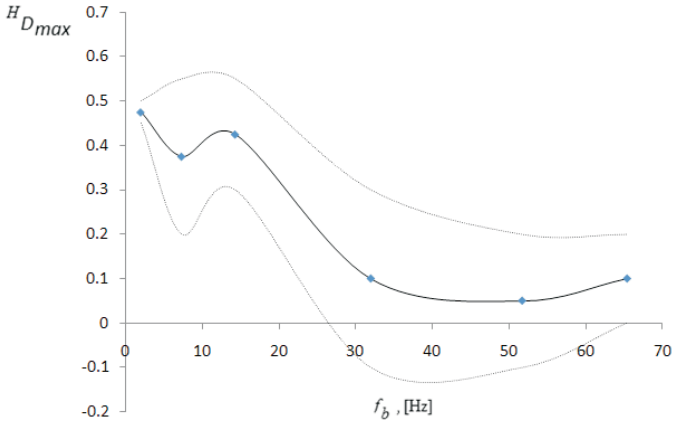

Figure 9. Hurst exponent vs. frequency of bubble departure. Calculation has been made using the libraries of LastWave [29,30] for 5 trajectories at different mean frequencies.

The value of H_{Dmax} characterizes the entire bubble path. For the low bubble departure frequencies (2, 7.3, 14.4 Hz) this value is close to 0.5 Hz and it means that bubble lateral mass centre displacements during the flow in the bubble column are ergodic, similarly to the Brownian motion. For $f_b > 30$ Hz the significant increase in the egrodic character of bubble lateral displacements has been observed.

This process can be explained as follows. When the frequency of bubble departure increases then the distance between bubbles in the column decreases. The strength of vorticities generated by previously departing bubbles increases. Such process leads to increase in egrodic character of the bubble path. The effect of influence of liquid flow generated by previously departing bubbles on the bubble trajectory is significant for $f_b > 30$ Hz. Taking this into consideration we can treat that the value of H_{Dmax} identifies the level of vertical interaction between bubbles.

5 Conclusions

In the paper the paths of bubbles emitted from the nozzle with frequency of bubble departure ranging from 2 Hz to 65.1 Hz have been analyzed. In case of low bubble departure frequency the typical behavior of bubble paths reported in other papers has been observed. For the higher frequencies of

bubble departure the decrease of lateral bubble displacement and length of rectilinear bubble movement after departure have been observed. It has been found that vertical terminal bubble velocity increases with the increase in frequency of bubble departures. The multifractal analysis shows that:

- Bubble paths have a multifractal character.
- Bubble lateral displacements during the flow in bubble column are ergodic, similarly to Brownian motion. The value of h_{max} would suggest non-random, correlated behavior at small scales horizontal displacements of bubbles.
- Influence of previously departing bubbles on multifractal characteristics of bubble trajectory in the column is significant for $f_b > 30$ Hz

As a turbulent flow has the multifractal character therefore the obtained multifractal character of bubble path confirms that bubble behaviors are connected with turbulent flow around the bubble. Obtained results show that the multifractal analysis can be a useful tool to analyze the dynamics of bubbles motion in the bubble column. It seems that it can be used to measure the strength of bubbles interaction in bubble columns.

Acknowlegment The authors are grateful for the financial support of Ministry of Science and Higher Education in Poland (Grant: N N503 138936).

Received 10 May 2010

References

[1] Luewisutthichat W., Tsutsumi A., Yoshida K.: *Chaotic hydrodynamics of continuous single-bubble flow system.* Chemical Engng Sc. **52**(1997), 3685–3691.

[2] Mosdorf R., Shoji M.: Chaos *in bubbling | nonlinear analysis and modelling.* Chemical Engng Sc. **58**(2003), 3837–3846.

[3] Zhang L., Shoji M.: *Aperiodic bubble formation from submerged orifice.* Chemical Engng Sc. **56**(2001), 5371–5381.

[4] Kikuchi R., *et al.*: *Diagnosis of chaotic dynamics of bubble motion in a bubble column.* Chemical Engng Sc. **52**(1997), 3741–3745.

[5] Femat R., Ramirez J.A., Soria A.: *Chaotic flow structure in a vertical bubble column.* Physics Letters A **248**(1998), 67–79.

[6] Vazquez A., Manasseh R., Sánchez R.M., Metcalfe G.: *Experimental comparison between acoustic and pressure signals from a bubbling flow.* Chemical Engineering Science **63**(2008), 5860–5869.

[7] Zenit R., Magnaudet J.: *Measurements of the streamwise vorticity in the wake of an oscillating bubble*. International Journal of Multiphase Flow **35**(2009), 195–203.

[8] Hedengren K.H.: *Decomposition of edge operators*. Proc. 9th International Conference on Pattern Recognition, Vol. 2, 14–17 Nov. 1988, 963–965.

[9] Shew W.L., Pinton J.F.: *Dynamical model of bubble path instability*. Physical Review Letters PRL **97**(2006) 144508.

[10] Peebles F.N., Garber H.J.: *Studies on the motion of gas bubbles in liquids*. Chem. Engng Progr. **49**(1953), 88–97.

[11] Hughes R.R., *et al.*: *The formation of bubbles at simple orifices*. Chem. Engng Progr. **51**(1955), 557–563.

[12] Davidson L., Amick E.: *Formation of gas bubbles at horizontal orifices*. AIChE J. **2**(1956), 337–342.

[13] Kling G.: *Über die Dynamik der Blasenbildung beim Begasen von Flüssigkeiten unter Druck*. Int. J. Heat Mass Transfer **5**(1962), 211–223.

[14] McCann D.J., Princ, R.G.H.: *Regimes of bubbling at a submerged orifice*. Chemical Engng Sc. **26**(1971), 1505–1512.

[15] Kyriakides N.K., Kastrinakis E.G., Nychas S.G.: *Bubbling from nozzles submerged in water: transitions between bubbling regimes*. Canadian J. Chemical Engng **75**(1997), 684–691.

[16] Davidson J.F., Schüler B.O.G.: *Bubble formation at an orifice in an inviscid liquid*. Trans. Instn. Chem. Engrs **38**(1960), 335–345.

[17] Zun I., Groselj J.: *The structure of bubble non-equilibrium movement in free-rise and agitated-rise condition*. Nuclear Engineering and Design **163**(1996), 99–115.

[18] Brenn G., Kolobaric, V., Durst F.: *Shape oscillations and path transition of bubbles rising in a model bubble column*. Chemical Engineering Science **61**(2006), 3795–3805.

[19] Sanada T., Sato A., Shirota M., Watanabe M.: *Motion and coalescence of a pair of bubbles rising side by side*. Chemical Engineering Science **64**(2009), 2659––2671.

[20] Sanada T., Watanabe M., Fukano T., Kariyasaki A.: *Behavior of a single coherent gas bubble chain and surrounding liquid jet flow structure*. Chemical Engineering Science **60**(2005), 4886–4900.

[21] Liu ZL., Zheng Y.: *PIV study of bubble rising behavior*. Powder Technology **168**(2006), 10–20.

[22] Auguste F., Fabre D., Magnaudet J.: *Bifurcations in the wake of a thick circular disk*. Theor. Comput. Fluid Dyn. **24**(2010), 305–313.

[23] Fabre D., Auguste F., Magnaudet J.: *Bifurcations and symmetry breaking in the wake of axisymmetric bodies*. Phys. Fluids **20**(2008) 051702.

[24] Ern P., Risso F., Fernandes P.C., Magnaudet J.: *Dynamical model for the buoyancy-driven zigzag motion of oblate bodies*. Physical Review Letters, PRL **102** (2009) 134505.

[25] Muzy J.F., *et al.*: *The multifractal formalism revisited with wavelets*. International Journal of Bifurcation and Chaos **4**(1994), 245–302.

[26] Enescu B.; Ito K., Struzik Z.R.: *Wavelet-based multiscale resolution analysis of real and simulated time-series of earthquakes*. Geophys. J. Int. **164**(2006), 63–74.

[27] Struzik Z.R.: *Determining local singularity strengths and their spectra with the wavelet transform*. Fractals **8**(2000), 163–179.

[28] Muzy J.F., *et al.*: *The multifractal formalism revisited with wavelets*. International Journal of Bifurcation and Chaos **4**(1994), 245–302.

[29] Mallat S.: *A Wavelet Tour of Signal Processing*. Academic Press, San Diego 1998.

[30] http://www.cmap.polytechnique.fr/∼bacry/LastWave/